This article has been accepted for publication in a future issue of this journal, but has not been fully edited. Content may change prior to final publication. Citation information: DOI 10.1109/TEC.2019.2956707, IEEE Transactions on Energy Conversion

A Dynamic Model of Small Modular Reactor-Based Nuclear Plants for Power System Studies

Bikash Poudel, *Student Member, IEEE,* Kalpesh Joshi, *Member, IEEE,* and Ramakrishna Gokaraju, *Senior Member, IEEE*

***Abstract*—Small modular reactors (SMRs), an emerging nuclear power plant technology, are suitable for large grids as well as remote load centers and offer load following and frequency response capabilities. While the SMRs have expectedly higher response rates, detailed dynamic models including reactor dynamics are necessary for power system dynamic studies. This paper presents a dynamic model of an integral pressurized water reactor (iPWR)-type SMR, modeled in Siemens PTI PSS/E, to assess the contribution of the reactor to the power system dynamics. The proposed SMR model mimics the heat generation process and subsequent heat transfer process with the inclusion of the reactor core based on point kinetics, primary coolant based on natural circulation, and a simplified three lump representation of the steam generator. Controllers are designed to operate the turbine valve and reactor control rod in closed loops. The SMR model is integrated with the modified turbine-governor system and a power system study is conducted. Results show the power system and internal reactor responses when subjected to electrical demand variations of 20% rated electrical output (REO) with a valve rate limit of ±80% REO/min.**

***Index Terms*—Nuclear power plant (NPP), Small modular reactor (SMR), Dynamic modeling, Integral pressurized water reactor (iPWR), Reactor dynamics, Governor response, Frequency response, Power system dynamic studies.**

NOMENCLATURE

This paper refers to conventional nuclear power plants as NPPs, and small modular reactor-based nuclear power plants as SMRs.

α_f, α_c	Fuel and moderator temperature coefficients of reactivity, (-2.16×10^{-5}, -1.8×10^{-4} /°C)
β	Delayed neutron fraction, (0.007)
$\dot{m}_{cp}, \dot{m}_{cs}$	Mass flow rate of primary coolant, secondary coolant, kg/s
$\dot{m}_{cp,0}$	Mass flow rate of primary coolant at rated SMR power, kg/s
η_T	Turbine efficiency
Λ	Prompt neutron lifetime, (2×10^{-5} s)
λ	Decay constant, (0.1 s^{-1})
μ_{max}, μ_{min}	Maximum and minimum valve position
ϕ	Average neutron flux, pu
ρ, ρ_{ext}	Net core reactivity, reactivity due to the control rod operation
τ	Fraction of thermal power in the fuel, (0.97)
A_{fc}	Effective heat transfer area: fuel to primary coolant, m^2
A_{pm}, A_{ms}	Effective heat transfer area: primary coolant to steam generator (SG) metal lump, SG metal lump to secondary coolant, m^2
c_m, c_{sw}, c_{sv}	Specific heat capacity of SG metal lump, saturated liquid in secondary of SG, saturated vapor in secondary of SG, $\mathrm{kJ/(kg\ °C)}$
c_{pf}, c_{pc}, c_p	Specific heat capacity of fuel lump, primary coolant lump in core region, primary coolant lump in SG, $\mathrm{kJ/(kg\ °C)}$
c_{pi}	Specific heat capacity of feedwater to the secondary of SG, $\mathrm{kJ/(kg\ °C)}$
h_{fc}, h_{pm}, h_{ms}	Heat transfer coefficient: fuel to coolant, primary coolant to SG metal lump, SG metal lump to secondary coolant, $\mathrm{W/(m^2\ °C)}$
K_P, K_I	Proportional, integral gain for rod control
m_c, m_p	Mass of primary coolant in the core region, primary coolant in SG region, kg
m_f, m_m	Mass of fuel lump, SG metal lump, kg
m_{HL}, m_{CL}	Mass of primary coolant in hot leg, in cold leg, kg
m_{sw}, m_{sv}	Mass of saturated liquid in secondary of SG, saturated vapor in secondary of SG, kg
P_0, P_{th}	SMR rated, instantaneous thermal power, MW(th)
P_{elec}	SMR electrical output, MW(e)
p_{sat}, p_{ref}, p_{in}	Saturated pressure at secondary of SG (steam pressure), reference pressure setpoint, pressure input of the flow model, MPa
R_{open}, R_{close}	Governor control for turbine valve opening, closing rate limits, % REO/min
T_f, T_m, T_{sat}	Average temperature of fuel, SG metal lump, secondary coolant lump in SG region, °C
T_p, T_{HL}, T_{CL}	Average temperature of primary coolant in SG region, hot leg, cold leg, °C
T_{c1}, T_{c2}	Average temperature of primary coolant at coolant node 1, coolant node 2, °C
T_{fi}	Feedwater inlet temperature, °C
U_w, U_v	Internal energy of saturated liquid and vapor in SG secondary, kJ/kg
v_w, v_v	Specific volume of saturated liquid and vapor in SG secondary, m^3/kg

Manuscript received August 12, 2019; revised October 12, 2019; accepted November 19, 2019. B. Poudel is a PhD student, K. Joshi is a PDF, and R. Gokaraju is a Professor in the Department of Electrical and Computer Engineering, University of Saskatchewan, Saskatoon, SK, Canada, e-mails: bikash.poudel@usask.ca; kalpesh.joshi@usask.ca; rama.krishna@usask.ca

Funding for this research was provided by the Sylvia Fedoruk Centre for Nuclear Innovation, Natural Sciences and Engineering Research Council (NSERC) Discovery Grant, and NSERC Engage Grant with Electranix Corporation, Winnipeg, Canada.

ΔT_f	Deviation in fuel temperature from initial steady state, °C
$\Delta T_{c1}, \Delta T_{c2}$	Coolant node 1, coolant node 2 temperature deviations from initial steady state, °C

I. Introduction

A recent study [1] shows that low-cost nuclear power can substantially reduce the average generation cost when a carbon constraint of 50 g CO_2/kWh or stricter is adopted. While nuclear power remains a strong contender as a provider of carbon-neutral electricity production for baseload generation [2], the smaller size and faster dynamics of small modular reactors (SMRs) make them potentially more suitable for flexible operations [3]–[6]. Historically, nuclear power plants (NPPs) in North America have been operated as baseload plants. However, NPPs in Europe have experienced flexible operation for both load following and frequency regulation for several years [7]–[9]. In the changing scenario of increasing share of intermittent generation from renewable energy sources, NPPs and SMRs are required to operate in flexible mode under which they may be subjected to large, sudden, and frequent variations in their electrical output.

While many models have been developed for different reactor types of conventional NPPs and advanced models are being developed for SMRs [10], very few attempts have been made to develop a model that adequately represents the reactor dynamics in electric grid-integration studies with an appropriate turbine model. Given that existing NPPs have limited participation in terms of absorbing demand fluctuations and grid disturbances, nuclear reactor dynamics is neither sufficiently represented nor integrated with the turbine-governor model in current power system simulation software packages.

The IEEE standard turbine-governor models approximate the internal source dynamics prior to the turbine valve and represent them with a first-order transfer function characterized by the charging time constant [11]. The steam pressure at the turbine inlet is assumed constant, and the mechanical power developed by the turbine is considered a linear function of the control valve position. This simplification works well with large interconnected systems in which each plant has a limited contribution to frequency regulation and balancing demand-generation. The inaccuracies, however, become apparent when the demand variations are large and the machines to regulate the frequency are fewer in number.

The need for dynamic models of NPPs and their important role in power system dynamic studies were highlighted in a number of past key IEEE PES publications, e.g., [12]–[15]. References [12], [13] present dynamic models of conventional NPPs for power system studies. Control strategies to improve the power maneuvering response were analyzed in [14], [15].

Recent publications such as [16] focus on small and slow changes, e.g., the NPP's response is limited to within 5% of its rated electrical output (REO) to the grid disturbance. The NPP model for a pressurized water reactor (PWR) plant in [16] uses a sliding average-temperature control program for the reactor with a simple turbine-governor model for grid integration. While the said NPP model represents the PWR in sufficient detail for power system studies, it was only tested for a small range of output variation with a limited ramp rate (30% REO/min). Other NPP models such as those in [17], [18], and [19] for grid-integrated studies have similar limitations of small and slow variations while including the nuclear reactor dynamics.

The 45 MWe NuScale SMR models developed in [20], [21] represent the reactor dynamics in finer detail, with consideration of primary coolant based on natural circulation and a moving boundary model of the steam generator (SG) with three distinct fluid state sections on the secondary side: the sub-cooled region, two-phase mixture, and the superheated region. The 100 MWe SMR model developed in [22] simplifies the thermodynamic relations of the reactor model for the purpose of controller design. All of the SMR models discussed have a sufficient level of accuracy based on their application, but none have attempted to integrate the dynamic model to the power system for power system dynamic studies.

Some NPPs in Europe operate in frequency control mode with ramp rates as high as 60% REO/min [8], [9]. The advanced controller design claims the possibility of ramp rates as high as 80% REO/min [22]. Further, the NERC guideline recommends the use of a GGOV1 turbine-governor model for grid-integrated generation plants [11], [23], and specifies different allowable frequency excursions for different regions [24]. Inaccuracies in frequency response during power system planning studies could lead to inadequate protection designs, hampering power system security.

In a nutshell, for the accurate and reliable representation of SMRs in power system studies, the following developments are required to bridge the existing research gaps:

1) A reactor model that can be integrated with the generic turbine model in power system dynamic simulations; and
2) Representation of reactor dynamics that can characterize the variation in prime-mover output during large and sudden fluctuations in electrical demand.

The authors' previous research works, [25], [26], investigate the power system aspect of having an SMR in an electrical grid, with [25] focusing on the power system's reliability to quantify the safety aspect of NPPs and [26] analyzing the steady-state power system issues of SMRs in a weak electrical grid. This paper aims to establish a dynamic model of an SMR to facilitate power system dynamic studies.

The paper is organized as follows. Section II describes the reactor model and integration with the turbine system. Section III discusses the reactor model performance and validation. Section IV utilizes the reactor model for power system simulation and shows the results for primary frequency control. Section V gives conclusions of the research work.

II. Reactor Modeling & Integration to Turbine

This section covers mathematical modeling of the 45 MWe NuScale SMR and its integration to the IEEE standard GGOV1 turbine-governor system.

Fig. 1 is a schematic diagram of a NuScale iPWR module. The reactor core consists of 37 standard 17×17 fuel assemblies with the core height almost half the height of a nominal PWR

This article has been accepted for publication in a future issue of this journal, but has not been fully edited. Content may change prior to final publication. Citation information: DOI 10.1109/TEC.2019.2956707, IEEE Transactions on Energy Conversion

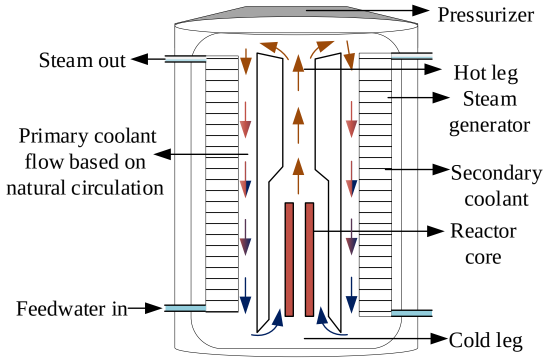

Fig. 1. Schematic diagram of NuScale iPWR module

[27]. The reactor core is equipped with two groups of control rod assemblies responsible for power regulation and shut down operations. The fuel is uranium dioxide (UO_2), with U-235 enrichment less than 4.95%. The primary coolant circuit is equipped with a pressurizer to keep the pressure within the reactor pressure vessel (RPV) constant during the operation. The primary coolant flow is based on natural circulation. Each reactor module consists of two, vertical, once-through, helical coil steam generators (HCSG) located between the hot leg riser and the external diameter wall [28]. Each steam generator comprises a total of 506 tubes forged with Inconel 690 alloy. Preheated feedwater enters through the lower plenum of the steam generator, where it boils after receiving heat from the primary coolant. The upper plenum of the steam generator delivers steam to the turbine units.

A. Reactor Core Model

The reactor core model incorporates the neutron dynamics inside the core, the thermal hydraulics responsible for the power transfer from the core to primary coolant, and the natural convection inside the primary coolant circuit. The pressurizer maintains the RPV pressure very close to the rated value even during large transients [29, p. 89], [30]. Moreover, the physical properties of the pressurized primary coolant are mainly influenced by the coolant temperature rather than the pressure. Therefore, the dynamics of pressurizer operation is neglected, and the RPV pressure is assumed to be constant. The coolant lumps are assumed well stirred with uniform temperature.

1) Reactor neutronic model: The core neutronics are described with the average neutron flux formulated as a point kinetics model consisting of a single energy model and a neutron precursor group obtained by combining six groups of delayed neutrons.

$$\frac{d\phi}{dt} = \frac{\rho}{\Lambda} - \frac{\beta}{\Lambda}\phi + \lambda C \tag{1}$$

$$\frac{dC}{dt} = \frac{\beta}{\Lambda}\phi - \lambda C \tag{2}$$

The net core reactivity (ρ) can be expressed as a summation of fuel and moderator temperature reactivity feedbacks and the reactivity due to the control rod operation.

$$\rho = \rho_{ext} + \alpha_f \Delta T_f + \alpha_c \frac{(\Delta T_{c1} + \Delta T_{c2})}{2} \tag{3}$$

2) Reactor thermal hydraulic model: Mann's model is adopted to describe the heat transfer process between a fuel lump and primary coolant [31]. Primary coolant in the core region is represented by two coolant nodes. The dynamic models of fuel and primary coolant temperatures in the reactor core region are expressed as

$$\frac{dT_f}{dt} = [\tau P_0 \phi + h_{fc} A_{fc}(T_{c1} - T_f)]/m_f c_{pf} \tag{4}$$

$$\begin{aligned}\frac{dT_{c1}}{dt} =& [(1-\tau)P_0\phi + h_{fc}A_{fc}(T_f - T_{c1})]/m_c c_{pc} \\ &+ 2\dot{m}_{cp}(T_{c1} - T_{c2})/m_c\end{aligned} \tag{5}$$

$$\begin{aligned}\frac{dT_{c2}}{dt} =& [(1-\tau)P_0\phi + h_{fc}A_{fc}(T_f - T_{c1})]/m_c c_{pc} \\ &+ 2\dot{m}_{cp}(T_{CL} - T_{c1})/m_c\end{aligned} \tag{6}$$

The temperature variation across the primary coolant circuit results in variation in the coolant density, thus creating the natural buoyancy force to vertically carry the coolant through the reactor core and hot leg riser. The primary coolant mass flow rate ($\dot{m}_{cp}$) based on the natural circulation can be expressed as a function of thermal power [20], as shown in (7).

$$\dot{m}_{cp} = \dot{m}_{cp,0} * \sqrt[3]{P_{th}/P_{th,0}} \tag{7}$$

3) Hot leg and cold leg: The average temperature of hot leg and cold leg regions can be expressed with first-order transfer functions:

$$\frac{dT_{HL}}{dt} = \frac{T_{c2} - T_{HL}}{\tau_{HL}}, \frac{dT_{CL}}{dt} = \frac{2T_P - T_{HL} - T_{CL}}{\tau_{CL}} \tag{8}$$

where $\tau_{HL} = \frac{\dot{m}_{cp}}{m_{HL}}$ and $\tau_{CL} = \frac{\dot{m}_{cp}}{m_{CL}}$.

B. Steam Generator Model

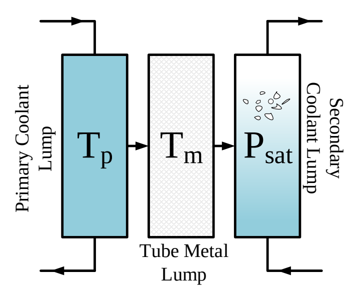

Fig. 2. Three lump representation of HCSG.

The H.B Robinson-based simplified three-lump SG Model A is adopted to represent the HCSG of the NuScale SMR [32, p. 27-39]. The model consists of three segments, representing primary coolant, tube metal, and secondary coolant, respectively. The heat transfer process between the coolant and metal tube is based on the average temperature of each lump. The secondary coolant lump is assumed to be in saturated condition with preheated feedwater entering the SG and saturated vapor coming out of it. The feedwater pumps and feedwater regulating valves continuously monitor and regulate the feedwater flow rate to keep up with the steam flow rate during normal and transient conditions [30], [33]. Perfect feedwater control

This article has been accepted for publication in a future issue of this journal, but has not been fully edited. Content may change prior to final publication. Citation information: DOI 10.1109/TEC.2019.2956707, IEEE Transactions on Energy Conversion

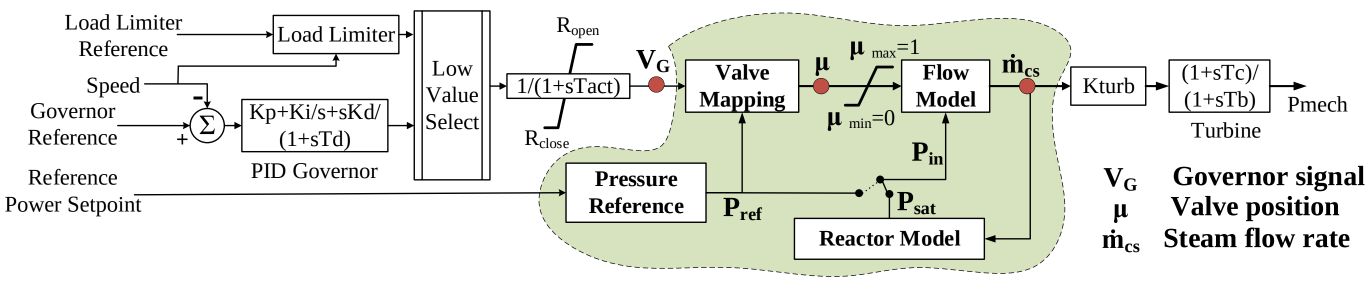

Fig. 3. GGOV1 modified and integrated with the SMR model; shaded region shows the modifications with new modules.

is assumed, which means the feedwater flow rate to the SG is always equal to the steam flow rate to the turbine.

Fig. 2 is a schematic diagram of the SG model. The secondary coolant lump is represented by its saturated pressure p_{sat}, whereas the primary coolant lump and the tube metal lump are represented by their average temperatures T_p and T_m, respectively. The thermodynamics of the SG is described by the following differential equations, obtained by combining mass and energy balance equations [32, p. 35-42].

$$\frac{dT_p}{dt} = K_{HL}(T_{HL} - T_p) + K_m(T_m - T_p) \tag{9}$$

$$\frac{dT_m}{dt} = K_{mp}(T_P - T_m) + K_{ms}(T_{sat} - T_m) \tag{10}$$

$$\frac{dP_{sat}}{dt} = \frac{K_{sm}(T_m - T_{sat}) - \dot{m}_{cs}(U_v - C_{pi}T_{fi})}{K_s} \tag{11}$$

where $K_{HL} = \frac{\dot{m}_{cp}}{m_p}$, $K_m = \frac{h_{pm}A_{pm}}{m_p c_p}$, $K_{mp} = \frac{h_{pm}A_{pm}}{m_m c_m}$, $K_{ms} = \frac{h_{ms}A_{ms}}{m_m c_m}$, $K_{sm} = h_{ms}A_{ms}$, $K_s = m_{sw}\frac{dU_w}{dp} + m_{sv}\frac{dU_v}{dp} - m_{sv}\frac{U_{wv}}{v_{wv}}\frac{dv_g}{dp}$, $U_{wv} = U_v - U_w$, and $v_{wv} = v_v - v_w$.

C. Integration to the Turbine-governor Model

The proposed dynamic model is integrated with the turbine system of a synchronous generator. The GGOV1 turbine-governor model is chosen for the integration because of the following advantages: the adjustable valve opening/closing rate limits; the governor can be controlled in isochronous or droop control mode; and load limiter signal can be customized and activated with reactor dynamic safety protocols.

The necessary modifications to the GGOV1 model to make it compatible with the proposed SMR model are illustrated in Fig. 3. The GGOV1 model assumes a constant steam pressure, and linear relationships between the governor signal, valve position, and mechanical output of the turbine. In the modified GGOV1, the governor signal is mapped to match the nonlinear valve model obtained from the International Atomic Energy Agency (IAEA)-based iPWR simulator [34]. The mapped signal represents the effective valve position at the SG outlet with the power change rate limits described by R_{open} and R_{close} settings. Fig. 4 shows the valve position corresponding to the governor signal for three different constant pressure setpoints.

The flow model takes the pressure and valve position as the inputs to calculate the steam flow. The flow model is equipped with an option to switch the pressure input p_{in} to reference pressure p_{ref} or steam pressure p_{sat}. For the simulation without considering the reactor, the flow model takes the valve position along with p_{ref}, based on the current power setpoint, thus acting as an inverse function of valve mapping and bypassing the reactor. When considering the reactor, p_{in} is switched back to p_{sat}, obtained from the reactor model.

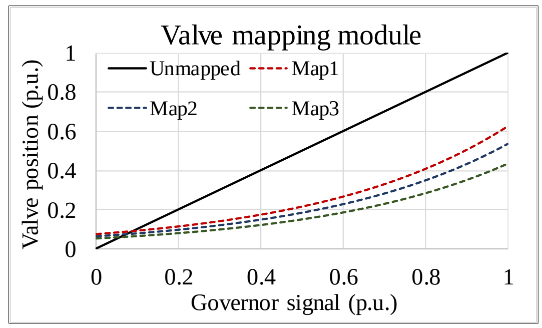

Fig. 4. Valve mapping process with p_{ref} corresponding to: Map1-100%, Map2-90%, and Map3-50% REO of SMR

III. Reactor Model Performance and Validation

Table I lists the major values used for the modeling. The primary coolant remains at a constant pressure of 12.46 MPa with different temperatures across the coolant circuit. The temperature of preheated feedwater in the secondary coolant circuit is kept constant at 170 °C.

Although the pressure of the secondary circuit varies with the reactor power level, the changes in the specific heat (c_{pi}) and internal energy of steam (U_v) are very small, and in fact the changes balance each other and the term $(U_v - c_{pi}T_{fi})$ in (11) is taken as a constant for the simulation. The mechanical power (P_{mech}) is a function of the enthalpy difference between the turbine inlet and outlet (Δh) and $\dot{m}_{cs}$, as shown in (12).

$$P_{mech} = \eta_T \Delta h \dot{m}_{cs} \tag{12}$$

During a power change, the variation in Δh is very small compared to the change in $\dot{m}_{cs}$. As a result, P_{mech} is taken as a function of $\dot{m}_{cs}$. The turbine efficiency η_T, on the other hand, varies with the steam flow rate. The relationship between η_T and $\dot{m}_{cs}$ is obtained from the iPWR simulator.

Constant average coolant temperature control mode is chosen as the control mode for the reactor. Fig. 5 shows the temperatures and steam pressure variations with respect to the

This article has been accepted for publication in a future issue of this journal, but has not been fully edited. Content may change prior to final publication. Citation information: DOI 10.1109/TEC.2019.2956707, IEEE Transactions on Energy Conversion

TABLE I
REACTOR CORE AND SG PARAMETERS [20] [21]

Fuel:	
Mass	11252 kg
Specific heat capacity	0.467 kJ/(kg °C)
Fuel to coolant:	
Heat transfer area	583 m^2
Heat transfer coefficient	1135 $\mathrm{W/(m^2\ °C)}$
Coolant volumes:	
Core region	1.879 m^3
Hot leg	9.7 m^3
Cold leg	26.8 m^3
SG primary	3.564 m^3
Primary coolant to SG:	
Heat transfer area	1123 m^2
Heat transfer coefficient	20391 $\mathrm{W/(m^2\ °C)}$
SG to secondary coolant:	
Heat transfer area	1214 m^2
Heat transfer coefficient	4950 $\mathrm{W/(m^2\ °C)}$
SG lump:	
Mass	7869 kg
specific heat capacity	0.450 kJ/(kg °C)

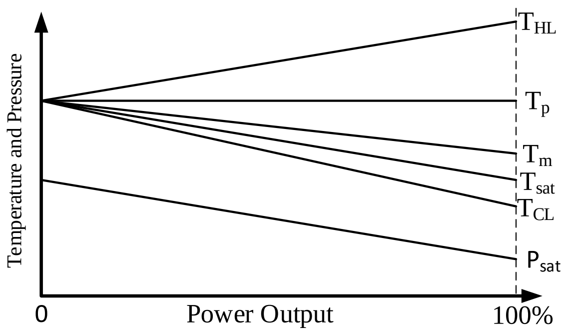

Fig. 5. Constant average coolant temperature control mode

change in reactor power. The positive slope of the hot leg temperature and the negative slope of the cold leg temperature ensure a constant average temperature while maintaining the temperature difference necessary for various power outputs. The secondary side pressure and temperature show decreasing trends for the increase in reactor power.

IAEA-based iPWR simulator software simulates the 45 MWe Nuscale iPWR module [34]. Steady-state setpoints of the modeled SMR are adjusted to obtain the steam pressure values equivalent to the ones obtained from the iPWR simulator. With these modeling principles, the model is developed as a user-defined model using the PSS/E software platform and Fortran programming environment. The overall reactor model is simulated in a steady state for various reactor power levels. The dynamic performance of an isolated reactor model is analyzed by simulating the reactor for step changes in valve opening and reactivity.

A. Steady-State Performance and Validation

The average primary coolant temperature setting of 252.5 °C is chosen for the proposed model because it provides a pressure range similar to that from the iPWR simulator [34]. The steady-state evaluation of the SMR model generates a power balance equation, (13), that represents the solution model for the power transfer between the primary and secondary coolant.

$$\frac{P_0\phi}{2m_pK_mc_{pc}} = T_p - T_m = \frac{K_{ms}\dot{m}_{cs}(U_v - c_{pi}T_{fi})}{K_{mp}K_{sm}} \tag{13}$$

The expression on the left-hand side represents the thermal power being transferred from the reactor core to the primary coolant; the expression on the right-hand side represents the thermal power transferred to the secondary coolant; and the middle expression relates the power terms with the temperature difference created. As T_p is kept constant at 252.5 °C, the power balance equation generates the solution in terms of T_m and ϕ for an electrical demand. All other variables of the reactor model are evaluated using the modeling equations in steady state. This steady-state evaluation provides the basis for setting up the initial conditions for the dynamic simulation.

TABLE II
SMR STEADY-STATE RESULTS FOR VARIOUS POWER LEVELS

P_{elec} (MWe)	$\dot{m}_{cs}$ (kg/s)	p_{sat} (MPa)	T_p (°C)	T_{HL} (°C)	T_{CL} (°C)	P_{th} (MWt)	T_f (°C)	$\dot{m}_{cp}$ (kg/s)
45	77.93	2.71	252.5	285.08	219.92	159.89	488.09	586.86
36	63.53	2.99	252.5	280.93	224.07	130.32	444.51	548.19
27	49.13	3.27	252.5	276.45	228.55	100.77	400.98	503.16
18	34.73	3.55	252.5	271.50	233.50	71.22	357.43	448.18
9	20.33	3.83	252.5	265.80	239.20	41.68	313.92	374.90
4.5	13.13	3.97	252.5	262.43	242.57	26.91	292.16	324.06

Table II lists some representative steady-state results obtained from the SMR model at different power levels. As the electrical demand decreases, the pressure and temperature of the secondary coolant increase. The reactor, on the other hand, readjusts the hot leg and cold leg temperatures while keeping the average temperature constant. Consequently, the temperature difference between the primary and secondary side decreases, thus reducing the thermal power transfer between the two sides and matching the new electrical demand.

B. Dynamic Performance of the Isolated SMR model

The SMR model is equipped with the provision of two control inputs necessary for power variation: reactivity and valve opening. To evaluate the isolated response of SMR to these two inputs, a step change in each variable is applied, with the results plotted in Fig. 6.

1) Response to step change in reactivity: With the help of the control rod, a 3.5×10^{-4} (i.e., 5¢) step increase in reactivity is applied at 20 s. The valve opening is left unchanged, and the core temperatures are allowed to drift in response to the change in thermal power. Following the step increase in reactivity, the reactor thermal power promptly increases due to the increased neutron flux. The fuel temperature and the primary coolant flow increase, followed by a rise in the temperature of the coolant lumps in the hot leg, steam generator, and cold leg regions. The average temperature of the primary coolant increases, leading to a larger temperature difference between the primary and secondary sides and thus increasing the heat transfer rate between the two sides. Because the valve position remains constant, the evaporation rate increases and leads to the rise in pressure and temperature of the secondary coolant.

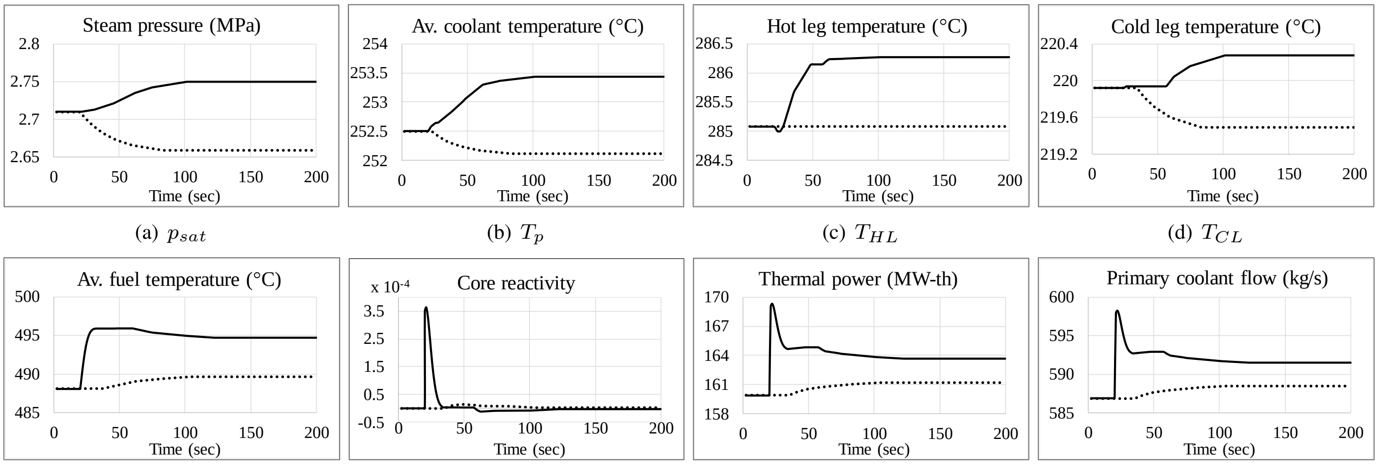

(a) p_{sat} (b) T_p (c) T_{HL} (d) T_{CL}

(e) T_f (f) ρ (g) P_{th} (h) $\dot{m}_{cp}$

Fig. 6. Dynamic responses for a step change in input variables. Solid lines represent the responses for 5% step increase in reactivity; dotted lines represent the responses for 10% step increase in valve opening.

On the reactor side, the reactivity feedback due to the rise in coolant temperature balances the reactivity due to the control rod movement. Finally, the reactor settles in a new steady-state condition with a 3.8 MW(th) increase in thermal power. The solid lines in Fig. 6 are the responses to a 5¢ step increase in reactivity.

2) Response to step change in valve opening: In the second case, a 10% step increase in valve opening is applied, while keeping the control rod inactive. The secondary coolant temperature and pressure decrease with the increase in valve opening. The decrease in temperature of secondary coolant leads to a larger temperature difference between the primary and secondary sides, thus increasing the heat transfer rate between the two sides. Because the control rod is disabled, the temperature of the primary coolant in SG region drops, leading to a decrease in cold leg temperature. The temperature of the primary coolant at the core region also decreases, thus increasing the net core reactivity. The increase in reactivity is followed by a small increase in thermal power, fuel temperature, and primary coolant flow rate. The reactivity feedbacks due to the increase in fuel temperature and decrease in coolant temperature balance each other. Due to this balancing effect, the hot leg temperature remains almost constant. Finally, the reactor settles in a new steady-state condition with a 1.31 MW(th) increase in thermal power. The dotted lines in Fig. 6 are the plots for the responses to a 10% step increase in valve opening.

IV. Power System Dynamic Studies with SMR

This investigation aims to incorporate the reactor dynamics into the power system dynamics and evaluate the flexibility of SMR to offer the primary frequency response. Fig. 7 depicts the power system model for the proposed dynamic study with the SMR model. The case system intends to mimic an isolated portion of the electrical grid in northern Canada. The system details are as follows: a 45 MWe, 13.8 kV SMR, stepped up to 33 kV to feed the load at the receiving end of a small 33 kV feeder. The line reactance is 0.03 pu, and transformer reactance is 0.08 pu, based on a 50 MVA system base.

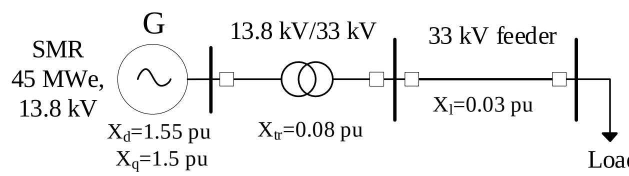

Fig. 7. SMR connected to a power system

Before integrating the SMR model with the power system model, the controllers should be appropriately designed to meet the power system requirements while respecting the design capability of the reactor. The two control variables are the reactivity and the valve opening, automated with the rod control system and the governor system, respectively. The governor control and rod control actuators are designed in such a way that the power maneuvering process completes smoothly under an extreme case scenario, which is taken as a 50% step decrease in electrical load.

A simple proportional-integral (PI) controller is designed to steer the control rod based on the deviation of average primary coolant temperature from the reference setpoint, as shown in (14).

$$\rho_{ext} = \left[K_P + \frac{K_I}{s}\right](T_p - T_{p,ref}) \qquad (14)$$

Four different control settings are considered and the valve control is set without any rate limits. Fig. 8(a) shows the reactor thermal power response corresponding to different control settings: $C1$: K_P=0.1, K_I=0.01; $C2$: K_P=0.05, K_I=0.005; $C3$: K_P=0.02, K_I=0.002; and $C4$: K_P=0.01, K_I=0.001. The control setting $C4$: K_P=0.01, K_I=0.001 ensures a smooth transition.

The governor control settings, R_{open} and R_{close}, limit the rate of valve operation. Three different rate limits are considered: (a) ±60% REO/min, (b) ±80% REO/min, and (c) no rate limits. The overshoot beyond 4 MPa in steam pressure

This article has been accepted for publication in a future issue of this journal, but has not been fully edited. Content may change prior to final publication. Citation information: DOI 10.1109/TEC.2019.2956707, IEEE Transactions on Energy Conversion

is considered a violation. Fig. 8(b) shows the steam pressure response for the three cases. Both $\pm 60\%$ and $\pm 80\%$ REO/min provide satisfactory response. Therefore, the valve rate limit of $\pm 80\%$ REO/min ($\pm 1.33\%$ REO/s) is selected.

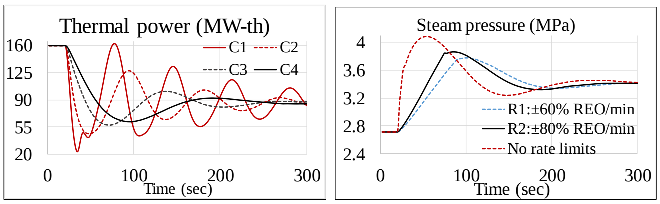

(a) (b)

Fig. 8. Responses: (a) Thermal power with rod control, (b) Steam pressure with different valve rate limits.

After designing the controllers for governor and rod control systems, the power system setup is simulated for electrical load demand changes. With the change in electrical load, the system frequency drifts from 60 Hz, and the governor will respond by operating the turbine valve to achieve the new demand. The governor system is controlled in isochronous mode, which will bring the system frequency back to the original 60 Hz. The turbine valve operation disrupts the power flow balance between the primary and secondary coolant. The control rod is steered to regulate the thermal power to reestablish the power balance. For primary frequency control, the SMR may opt to operate without the control rod movement. Power adjustments without the control rod for up to 25% REO are seen occasionally, even for conventional NPPs [35].

The total simulation time is 600 s. The electrical load changes from 100% to 80% REO of the SMR at 20 s. The system is allowed to settle until 400 s. At 400 s, a 20% step increase brings the load back to 100% REO of SMR. Load step changes of $\pm 20\%$ REO are considered here to evaluate the reactor model for an extreme case scenario of primary frequency control. In actual practice, the frequency disturbances would be smaller and, SMR may also share the demand fluctuations with other flexible power sources.

Power system dynamics in this investigation is assessed in terms of the maximum frequency deviation and frequency recovery time. The frequency recovery within ± 0.5 Hz is considered a recovered state or a no trip zone, which also mimics the NERC standard for frequency relays for generators [11], [24]. As the simulation assumes an isolated configuration with large step changes in electrical load, the frequency deviations are bound to be much larger than in actual practical scenarios.

Three cases are considered: Case I-without reactor, Case II-with uncontrolled reactor, and Case III-with controlled reactor. The power system responses are plotted in Fig. 9. The reactor side responses are plotted in Fig. 10.

A. Case I-Without Reactor

Case I is activated by switching the pressure input p_{in} of the flow model in Fig. 3 to p_{ref}. The turbine-governor model with valve rate limit of $\pm 80\%$ REO/min replicates the design limit of SMR to offer the power variation. The zoomed section of the frequency response in Fig. 9(a) shows the frequency response corresponding to the step decrease in load at 20 s. The frequency overshoot in Case I is 62.873 Hz, while the frequency recovers at T1(=43 s) of the simulation. A similar trend is seen for the load step increase occurring at 400 s. As the reactor model is kept inactive for Case I, the reactor side responses are not available.

B. Case II-With Uncontrolled Reactor

The reactor model is activated by switching p_{in} of the flow model back to p_{sat}. The control rod system is disabled; thus, the average coolant temperature will not remain constant. The change in thermal power occurs due to the temperature feedback on core reactivity. Because the reactor model is activated, the flow model receives variable pressure from the reactor model. When the load demand decreases at 20 s, the valve closes and leads to an increase in steam pressure, which in turn necessitates the valve to close even more to match the new load demand. The case is worsened when the reactor is not controlled to maintain the average coolant temperature, causing the steam pressure to rise even more. The temperature of the primary coolant increases, decreasing the net core reactivity. The reactor thermal power and fuel temperature decrease, and the reactor settles when the reactivity feedbacks due to the decrease in fuel temperature and increase in coolant temperature balance each other. The steam pressure settles at 3.37 MPa, while the system thermal power settles with a net decrease of 26.98 MW(th) as shown in Fig. 10(e). With a bigger change in valve opening, shown in Fig. 9(c), the turbine takes more time to achieve the new mechanical power. Consequently, the frequency response will be slower with a frequency recovery time of T2(=81 s), as shown in Fig. 9(a). The frequency overshoot is 63.107 Hz. A similar trend is seen for the load step increase occurring at 400 s.

C. Case III-With Controlled Reactor

The control rod system is activated, and the reactivity of the core is controlled to maintain the average primary coolant temperature constant. When the load decreases at 20 s, the valve closes and causes an increase in steam pressure. However, due to the control rod insertion, the core reactivity decreases, reducing the thermal power, average fuel temperature, and primary coolant flow rate. As a result, the hot leg temperature decreases, keeping the average coolant temperature constant. The steam pressure recovers and settles at 2.99 MPa as shown in Fig. 10(a). The pressure recovery allows the turbine to achieve the new mechanical power at a higher valve position, thus reducing the change required in valve position. Fig. 9(a) shows the frequency recovery time is T3(=70 s), while the frequency overshoot is 63.107 Hz. The thermal power settles with a net decrease of 28.1 MW(th), as shown in Fig. 10(e).

D. Comparison

In Case I, the reactor dynamics was not considered and, as a result, the electrical side responses had inaccuracies. The frequency overshoot was 0.234 Hz less than the other

This article has been accepted for publication in a future issue of this journal, but has not been fully edited. Content may change prior to final publication. Citation information: DOI 10.1109/TEC.2019.2956707, IEEE Transactions on Energy Conversion

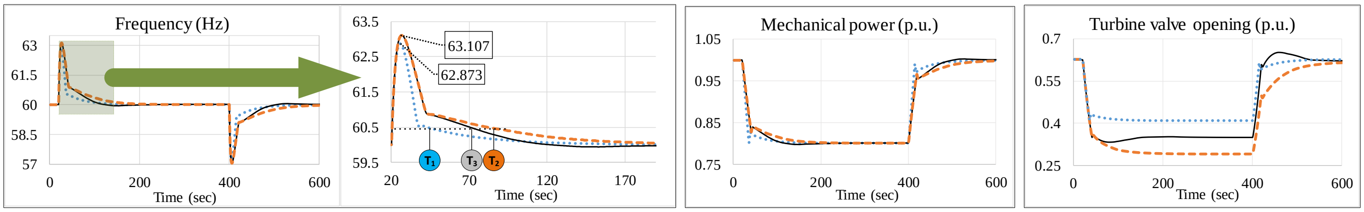

(a) Frequency: fullscale and zoomed section (b) P_{mech} (c) μ

Fig. 9. Power system dynamic responses for step changes in electrical demand. Legends: Case I(.....), Case II(- - -), Case III(—).

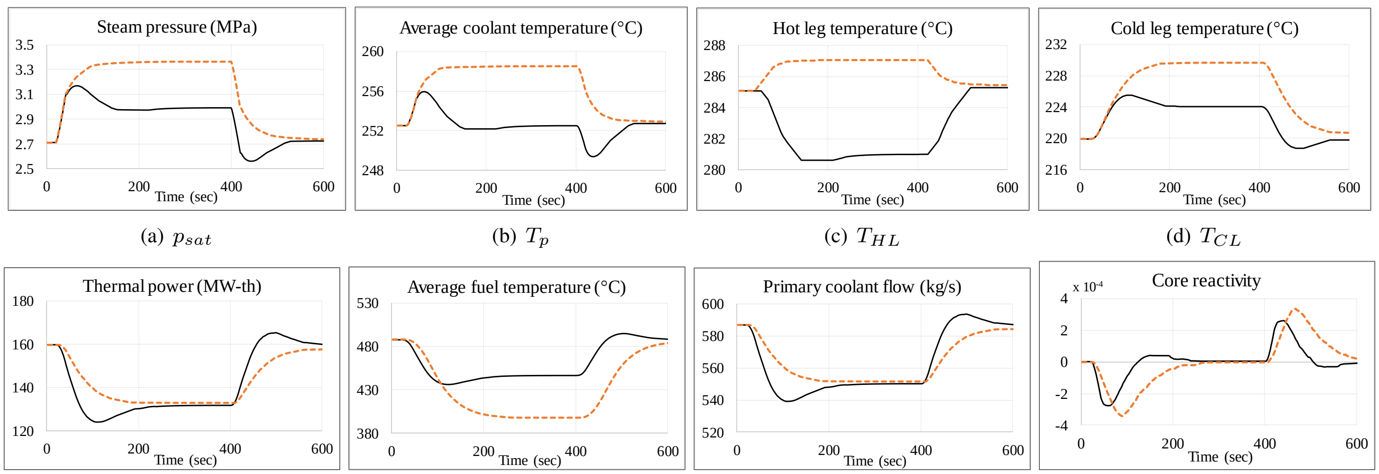

(a) p_{sat} (b) T_p (c) T_{HL} (d) T_{CL}

(e) P_{th} (f) T_f (g) $\dot{m}_{cp}$ (h) ρ

Fig. 10. Reactor dynamic responses for step changes in electrical demand. Legends: Case II(- - -), Case III(—).

two cases, and the frequency recovery time was 38 and 27 s less than in Case II and Case III, respectively. In Case II, the frequency response was obtained without control rod operation. Although the frequency overshoot was about the same, the frequency recovery time was 11 s slower compared to Case III for the same electrical disturbance. The change in steam pressure was 0.38 MPa more than in Case III. Similarly, the overshoot in core reactivity, variation of fuel temperature, and range of primary coolant temperature were significantly more for Case II. These results indicate the range of power variation possible with an uncontrolled reactor is considerably less than with a controlled reactor. The controlled reactor-based frequency response is, therefore, faster, more stable, and relatively safer than the uncontrolled case.

V. Conclusion

This paper proposed a dynamic model of an iPWR-type SMR to facilitate the inclusion of SMR dynamics in power system dynamic studies. The SMR model included the heat generation process based on point kinetics, RPV thermal hydraulics based on natural circulation, and a simplified three lump representation of SG. The generic GGOV1 turbine-governor model was modified with a valve mapping module to incorporate the steam pressure variation from the reactor. A power system dynamic study was conducted to evaluate the contribution of the reactor dynamics in power system frequency response. The results showed the power system and reactor responses for a 20% step change in electrical load for three different cases: without reactor, with uncontrolled reactor, and with controlled reactor. The comparisons showed the significance of an accurate SMR model for power system dynamic studies and the necessity of reactor control for primary frequency regulation.

Acknowledgments

The authors would like to thank Mr. Dennis Woodford, Electranix Corporation for the valuable feedback he provided on the research. The authors also would like to thank Prof. Esam Hussein, University of Regina for the leadership he provided for the overall Fedoruk Center project. The constructive comments provided by the anonymous reviewers' on the paper are sincerely appreciated. The authors thank IAEA, Vienna, Austria, for providing the iPWR SMR simulator.

References

[1] J. Buongiorno, M. Corradini, J. Parsons, and D. Petti, "Nuclear energy in a carbon-constrained world: Big challenges and big opportunities," *IEEE Power and Energy Magazine*, vol. 17, no. 2, pp. 69–77, Mar 2019.

[2] International Energy Agency, "World energy outlook 2014, executive summary," International Energy Agency, Paris, France, Tech. Rep., 2014. [Online]. Available: www.iea.org

[3] C. Alexander Glaser, M. Ramana, A. Ahmad, et al.,"Small modular reactors a window on nuclear energy an energy technology distillate," Andlinger Center for Energy and the Environment, Princeton University, Princeton, Tech. Rep., 2015. [Online]. Available: http://acee.princeton.edu/distillates.

[4] J. Jenkins, Z. Zhou, R. Ponciroli, R. Vilim, F. Ganda, F. de Sisternes, and A. Botterud, "The benefits of nuclear flexibility in power system operations with renewable energy," *Applied Energy*, vol. 222, pp. 872–884, Jul 2018.

This article has been accepted for publication in a future issue of this journal, but has not been fully edited. Content may change prior to final publication. Citation information: DOI 10.1109/TEC.2019.2956707, IEEE Transactions on Energy Conversion

[5] D. T. Ingersoll, C. Colbert, Z. Houghton, R. Snuggerud, J. W. Gaston, and M. Empey, "Can nuclear power and renewables be friends?" in *Proceedings of ICAPP*, Nice, France, May 2015, pp. 1–9.

[6] C. Marcinkiewicz, "Nuscale small modular reactors: Advanced, scalable, flexible, economic," PNWER Energy Working Group Presentation, July 2017.

[7] S. Feutry, "Load following and frequency control transients - edf experience and practice," in *IAEA Technical Meeting on Flexible Operation Approaches of Nuclear Power Plants*. Paris, France: International Atomic Energy Agency, September 2013.

[8] Nuclear Energy Agency, "Technical and economic aspects of load following with nuclear power plants," Tech. Rep. June, 2011.

[9] International Atomic Energy Agency, "Non-baseload operation in nuclear power plants: Load following and frequency control modes of flexible operation," Vienna, Austria, Tech. Rep. NP-T-3.23, 2018.

[10] G. Li, X. Wang, B. Liang, X. Li, B. Zhang, and Y. Zou, "Modeling and control of nuclear reactor cores for electricity generation: A review of advanced technologies," *Renewable and Sustainable Energy Reviews*, vol. 60, pp. 116–128, Jul 2016.

[11] Task Force on Turbine-Governor Modeling, "Dynamic models for turbine-governors in power system studies," IEEE Power and Energy Society, Tech. Rep. PES-TR1, 2013.

[12] T. Ichikawa and T. Inoue, "Light water reactor plant modeling for power system dynamics simulation," *IEEE Transactions on Power Systems*, vol. 3, no. 2, pp. 463–471, May 1988.

[13] T. Inoue, T. Ichikawa, P. Kundur, and P. Hirsch, "Nuclear plant models for medium- to long-term power system stability studies," *IEEE Transactions on Power Systems*, vol. 10, no. 1, pp. 141–148, Feb 1995.

[14] Q. B. Chou, P. Kundur, P. N. Acchione, and B. Lautsch, "Improving nuclear generating station response for electrical grid islanding," *IEEE Transactions on Energy Conversion*, vol. 4, no. 3, pp. 406–413, Sep. 1989.

[15] T. D. Younkins, J. R. Winkelman, J. J. Sanchez-Gasca, and J. A. McGrady, "Output feedback multivariable control for an advanced boiling water reactor," *IEEE Transactions on Energy Conversion*, vol. EC-2, no. 3, pp. 349–354, Sep. 1987.

[16] S. E. Arda and K. E. Holbert, "Implementing a pressurized water reactor nuclear power plant model into grid simulations," in *2014 IEEE PES General Meeting | Conference Exposition*, July 2014, pp. 1–5.

[17] L. Xiong, D. Liu, B. Wang, P. Wu, J. Zhao, and X. Shi, "Dynamic characteristics analyse of pressurized water reactor nuclear power plant based on PSASP," *2009 4th IEEE Conference on Industrial Electronics and Applications, ICIEA 2009*, pp. 3629–3634, 2009.

[18] H. Gao, C. Wang, and W. Pan, "A detailed nuclear power plant model for power system analysis based on PSS/E," *2006 IEEE PES Power Systems Conference and Exposition, PSCE 2006 - Proceedings*, pp. 1582–1586, 2006.

[19] S. E. Arda, K. E. Holbert, and J. Undrill, "Development of a linearized model of a pressurized water reactor generating station for power system dynamic simulations," in *2013 North American Power Symposium (NAPS)*, Sep. 2013, pp. 1–6.

[20] S. E. Arda and K. E. Holbert, "A dynamic model of a passively cooled small modular reactor for controller design purposes," *Nuclear Engineering and Design*, vol. 289, pp. 218–230, 2015.

[21] ——, "Nonlinear dynamic modeling and simulation of a passively cooled small modular reactor," *Progress in Nuclear Energy*, vol. 91, pp. 116–131, 2016.

[22] D. Bose, S. Banerjee, M. Kumar, P. P. Marathe, S. Mukhopadhyay, and A. Gupta, "An interval approach to nonlinear controller design for load-following operation of a small modular pressurized water reactor," *IEEE Transactions on Nuclear Science*, vol. 64, no. 9, pp. 2474–2488, 2017.

[23] L. Pereira, J. Undrill, D. Kosterev, D. Davies, and S. Patterson, "A new thermal governor modeling approach in the WECC," *IEEE Transactions on Power Systems*, vol. 18, no. 2, pp. 819–829, May 2003.

[24] NERC, "NERC standard PRC-024-2 - Generator frequency and voltage protective relay settings," pp. 1–12.

[25] B. Poudel, K. Joshi, and R. Gokaraju, "An approach to assess reliability of offsite power as site selection criteria for a nuclear power plant," in *38th Annual Conference of the Canadian Nuclear Society and 42nd Annual CNS/CNA Student Conference*, Saskatoon, Canada, June 2018, pp. 1–6.

[26] B. Poudel, K. A. Joshi, and R. Gokaraju, "Analysis for siting and sizing of a small modular reactor – a case study in canada," in *20th National Power System Conference*, Tiruchirappalli, India, Dec 2018, pp. 1–6.

[27] "Final Safety Analysis Report (Rev. 2) - Part 02 - Chapter 04 - Reactor," NuScale Power LLC, Corvallis, Oregon, Tech. Rep. October, 2018.

[28] "Final Safety Analysis Report (Rev. 2) - Part 02 - Chapter 05 - Reactor Coolant System and Connecting Systems," NuScale Power LLC, Corvallis, Oregon, Tech. Rep. October, 2018.

[29] S. E. Arda, "Nonlinear dynamic modeling and simulation of a passively cooled small modular reactor," Doctoral Dissertation, Arizona State University, 2016. [Online]. Available: https://repository.asu.edu/items/40760

[30] G. Wu, P. Ju, X. Song, C. Xie, and W. Zhong, "Interaction and coordination among nuclear power plants, power grids and their protection systems," *Energies*, vol. 9, no. 4, p. 306, 2016.

[31] T. W. Kerlin, E. Katz, J. G. Thakkar, and J. E. Strange, "Theoretical and experimental dynamic analysis of the H. B. robinson nuclear plant," *Nuclear Technology*, vol. 30, no. 3, pp. 299–316, 1976.

[32] M. R. A. Ali, "Lumped parameter , state variable dynamic models for u-tube recirculation type nuclear steam generators," PhD Dissertation, University of Tennessee, Knoxville, 1976.

[33] "Final Safety Analysis Report (Rev. 2) - Part 02 - Chapter 10 - Steam and Power Conversion System," NuScale Power LLC, Corvallis, Oregon, Tech. Rep. October, 2018.

[34] C. Batra, *Integral Pressurized Water Reactor Simulator Manual*. International Atomic Energy Agency, 2018, vol. 1.

[35] L. E. Weaver, "Reactor control," in *Nuclear Power Safety*, J. H. Rust and L. E. Weaver, Eds. Oxford: Pergamon, 1976, pp. 169 – 208.

Bikash Poudel (S'17) received the Bachelor's degree in Electrical Engineering (with Distinction) from the Tribhuvan University, Nepal, in 2014. During 2015-2016, he worked as an Assistant Lecturer in Kathmandu Engineering College, Nepal. He joined the department of Electrical and Computer Engineering, University of Saskatchewan for graduate studies in Sept 2016 and is currently working towards the PhD degree. His research interests include the dynamic modeling of nuclear power plants and renewable energy sources, and power system dynamics.

Kalpesh Joshi (M'12) received his Ph.D. degree in Electrical Engineering from the Indian Institute of Technology Gandhinagar in 2017 and M.Tech. degree in Power Systems from the Indian Institute of Technology Delhi, India, in 2008. Receiving the prestigious post-doctoral fellowship from the Shastri Indo-Canadian Institute (SICI), he worked as a post-doctoral researcher in the department of Electrical and Computer Engineering at the University of Saskatchewan, Canada for two years. He has also worked as a visiting research scholar with the Washington State University, Pullman, USA in 2015. Joshi's research interests include modeling, analysis and optimization of distribution networks with distributed generation, energy storage systems and advanced small modular (nuclear) reactors. He is also interested in the protection and control aspects of active distribution networks and micro grids.

Ramakrishna Gokaraju (S'88, M'00, SM'15) received his Bachelor of Engineering degree (with Distinction) in Electrical and Electronics Engineering from the National Institute of Technology, Trichy, India in April 1992. He received the M.Sc. and Ph.D. degrees in electrical and computer engineering from the University of Calgary, Calgary, AB, Canada, in 1996 and 2000, respectively. During 1999-2002, he was a Research Scientist with the Alberta Research Council and a Staff Software Engineer with IBM Toronto Lab. He joined the Department of Electrical & Computer Engineering at the University of Saskatchewan as an Assistant Professor in 2003 and is currently a professor in the department. His current research works are in high speed digital relaying, controlled islanding, fault detection in dc systems, impact of inverter based resources on protection, and dynamic modeling of nuclear-based ("SMR") power plants.